

A simplified structural mechanics model for cable-truss footbridges and its implications for preliminary design



Zhijun Chen^a, Hongyou Cao^a, Hongping Zhu^a, Jun Hu^a, Shaofan Li^{a,b,*}

^a School of Civil Engineering & Mechanics, Huazhong University of Science & Technology, Wuhan 430074, China

^b Department of Civil and Environmental Engineering, University of California, Berkeley, CA 94720, USA

ARTICLE INFO

Article history:

Received 13 May 2013

Revised 22 February 2014

Accepted 24 February 2014

Available online 27 March 2014

Keywords:

Cable-truss footbridge

Finite element analysis

Structural mechanics model

Structural optimization

Suspension bridge

ABSTRACT

Compared with traditional suspension footbridges, the cable-truss footbridge is always easier to satisfy structure deformation requirements under small dead-load-to-live-load ratio condition, and it enjoys surging popularity in western China. In this type of bridges, the deck system is designed as a pure local load-bearing member, and the inverse pre-tensioned deck cable system is set up to form a tension–tension mechanical system. To better understand its structural performance, a simplified structural mechanics model for cable-truss footbridges is proposed, and the analytical formulations for deformation and internal forces of the bridge under entire span live load as well as semi-span live load have been derived. The reliability and accuracy of the proposed model have been validated in a comparison study with the finite element analysis. Furthermore, a series of qualitative and quantitative parametric studies have been conducted, which reveal that the cable-truss bridges have several novel structural characteristics that differ from that of traditional suspension bridges. Finally, the affordability range of cable-truss bridges is also discussed by using material usage analysis.

© 2014 Elsevier Ltd. All rights reserved.

1. Introduction

With emergence of new materials, advanced structural engineering technology, and demands of larger spans in bridge and building structures in modern society, more and more cable-supported structures are being built due to their light weight, high strength, ease of construction, and aesthetic appearance. In recent years, many novel structure types of cable supported footbridges have been built or designed, such as ribbon footbridges, tensegrity-based footbridges, and suspension footbridges with a reverse profiled pre-tensioned cable e.g. [12,18], and [22]. However, due to its small dead-load-to-live-load ratio, no matter what geometric configuration of the bridge is, large span cable supported footbridge always suffers the shortcomings due to its intrinsic characteristics being slender and flexible, this makes it prone to vibration induced by functional activities or wind loads. Accordingly, pedestrian or wind-induced vibrations have become a focal point in the cable-supported footbridge design and research e.g. [27,6,23], and [15]. Obviously, increasing suspension footbridge's deck or girder stiffness is one of the best ways to improve the structure's load

bearing capacity. However, this approach will increase the overall dead-load-to-live-load ratio, and hence it is often expensive. Therefore instead of increasing footbridge's deck/girder stiffness, researchers have attempted to enhance the load bearing capacity as well as dynamic performance of the bridge by modifying the hanger system, such as adding stay cables, and so on, e.g. [24,13,8]. Among of them, an effective approach to enhance the suspension bridge's overall stiffness and to control the bridge's deformation amplitude under external loads is to add an inverse pre-tensioned cable below the bridge deck to form a cable-truss structure (see Fig. 1(a) and (b)), and this technique was originated from the cable-truss roof construction. The cable-truss footbridge is composed of a bi-concave cable and tension hangers, whereas conventional cable-truss structures are usually designed to be composed of a bi-convex cable and compression struts. Compared to traditional suspension bridges, the deck system in a cable-truss footbridge can be designed solely as a local load-bearing member, whose vertical stiffness is very small so that it can be neglected in the mechanical analysis; the prestressed reverse profiled cable is set up to share the load and to enhance the overall stiffness of the bridge. This form of structure is also called cable-truss beam developed by Swedish engineer, David Jawerth in the 1960s (see: Buchholdt [2]), and then this structural system was late applied to roofs (Fig. 1c) and footbridges by other engineers such as Majowiecki [21], Schlaich and Englesmann [11], and Strasky [12] and

* Corresponding author at: Department of Civil and Environmental Engineering, University of California, Berkeley, CA 94720, USA. Tel.: +1 510 642 5362; fax: +1 510 643 8928.

E-mail address: li@ce.berkeley.edu (S. Li).

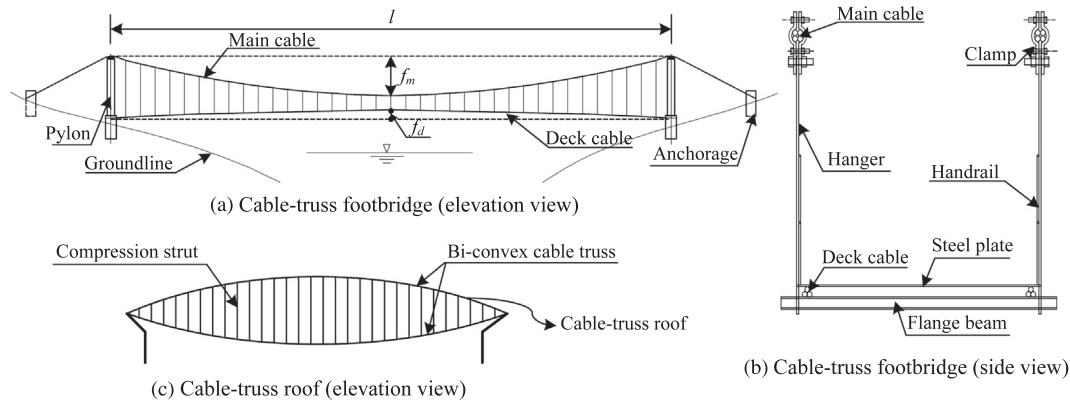


Fig. 1. Cable-truss structures.

others. Zetlin's Municipal Auditorium in Utica, New York was the first cable-truss structure, and comprehensive analytical treatments of cable-truss structures used in buildings were given by Schleyer and Møllmann (see: Irvine [9]), and then some celebrated roof structures including David L. Lawrence Convention Center in Pittsburgh, PA, Chonju World Cup Stadium in Korea, and an exhibition hall for the Hanover Fair [14] also adopted similar structural design. After that, reverse profiled cables have been extensively used to enhance the lateral stiffness of suspension bridges, such as the M-bridge built in 1999 [28].

Huang et al. [19,20] proposed a shallow suspension footbridge with reverse profiled pre-tensioned cables, and conducted a series of studies examining the deformation and vibration characteristics of this type of footbridge by using finite element method. To reduce cable's shape change under the action of non-uniform loads, Goremikins et al. [30] replaced the main cable by a cable truss beam with cambered top and bottom chords and inclined web element, where all truss elements are tensioned, and subsequently their vertical displacements are reduced. In general, the application and research of cable-truss structure on bridge engineering lags relatively behind to those of roof structures.

Cable-truss structure is a complex structural form with strong nonlinearity. As the development of finite element method, nonlinear finite element method has been extensively used to analyze mechanical strength and performance of cable-truss structures [17,16,30]. However, in preliminary/conceptual designs, a relatively simple analytical method can provide a reasonable and quick estimate for structural engineers in analysis and design of cable-truss bridges. As mentioned above, comprehensive analytical treatments of cable-truss structures used in buildings were given by Schleyer and Møllmann [9]. They neglected all the second-order terms in the differential equations of both cable equilibrium and compatibility conditions to obtain a linearized approximation theory to analyze static responses of cable-truss structures under external loads. This method also had been adopted in the some later works, e.g., Baron and Venkatesan [5], Urelius and Fowler [29] and Buchholdt [2]. Monforton and El-Hakim [7] used the energy method to analyze pin-ended cable-truss structures. In this work, both geometric and material nonlinearities are directly incorporated within the structural mechanics formulation. Recently, Kmet and Kokorudova [25,26] have proposed a more sophisticated structural mechanics model for cable-truss structures. They kept the high-order terms neglected in the linearized approximation theory mentioned above, and considered a suspended biconvex and biconcave cable-truss with unmovable, movable, or elastic yielding supports subjected to vertical distributed loads applied over the entire or semi span. The proposed mathematical model for

cable-truss structure is derived on the basis of initial cable shape and the structure response that was obtained from the load equilibrium equations and cable compatibility equations. And all of the methods mentioned above assumed that the hangers are arranged vertically and inextensible.

In this paper, a novel structural mechanics model for cable-truss bridges under either entire or semi span loading is proposed. Different from the previous cable-truss bridge models, whose solutions require the load conditions of two different cases, the structure's deformed configuration is determined at first in terms of mid-span sag and external load parameters, and then the cable compatibility equations are used to acquire the mid-span sag. By this way, the derivations are greatly simplified. During the derivations, some approximations or assumptions are being made, which are similar to that of the existing models. Even though, for long span footbridge, the pedestrian or wind induced vertical or transverse vibration are important issues, and they have attracted the much attention of many researchers e.g. Taylor and Vezza [10], Fiore and Monaco [1], Ingólfsson and Georgakis [4]. However, these factors are not considered in the proposed model, because the objective of this paper is to build a simple model for preliminary/conceptual static design. The reliability and accuracy of the proposed model is validated through a comparison study with the nonlinear finite element method. Besides these studies, a systematic parameter analysis has been performed to investigate the stiffness relationship between the main cable and deck cable according to different dead or live load conditions. The optimal analysis was also conducted to determine the affordability range for cable-truss bridges, which is depended on the load conditions and material strength.

2. Mechanics model for single cable structures

First, it is necessary to establish a single cable statics model, which can serve as the basis of the cable-truss bridge model. An exact analysis of simply suspended cable problems is somewhat restricted because the solution methods are cumbersome. Simplifications can be made when the profile of the cable is flat, and this often corresponds to situations in which cables with relatively low sag are used for structural purposes. The approximation method based on parabola theory provides explicit and consistent methods for finding the static response to applied loads that are accurate to the third order of small quantities [9]. All of the derivations in this paper are based on structural mechanics and analytic geometry instead of energy approaches. The following assumptions are made for the derivation of the mathematical governing equations:

- (1) The bridge is subjected to a uniformly distributed dead load including deck load and weight of cables and hangers.
- (2) The cable configuration is parabolic based on the first assumption.

2.1. Expression of a single cable's configuration

Based on Assumption 1 and by using the notations shown in Fig. 2, the deformed configuration of the cable can be found when the supports are at the same level according to the solution of an analogous simply supported beam model with the same span subjected by the same external load [24].

The cable configuration, as shown in Fig. 2, may be expressed as

$$y = -\frac{M(x)}{H} \quad (1)$$

where $M(x)$ and H represent the bending moment distribution of the simply supported beam and the horizontal force of the cable respectively.

Based on Eq. (1) and Assumption 1, the following cable profile equations under the three different load cases shown in Fig. 2 can be derived:

$$y = \frac{f}{a^2}x(x - 2a) \quad (\text{Dead load}) \quad (2)$$

$$y = \frac{f_1}{a^2}x(x - 2a) \quad (\text{Load case 1}) \quad (3.1)$$

$$y = \begin{cases} \frac{2(p+w)x^2 - (3p+q+4w)ax}{(p+q+2w)a^2} f_2 & (0 \leq x \leq a) \\ \frac{2(q+w)x^2 - (5q+4w-p)ax - 2(p-q)a^2}{(p+q+2w)a^2} f_2 & (a < x \leq 2a) \end{cases} \quad (\text{Load case 2}) \quad (3.2)$$

where f , f_1 , and f_2 are the sag of the cable at the mid-span for the dead load, load case 1, and load case 2, respectively; w is the uniform dead load, including the weight of the cable and deck system; p and q are the external loads acting on the different semi-spans. The equation for the deformed cable configuration as expressed in Eqs. (3.1) and (3.2) are in terms of one or both of the new mid-span sag and load parameters (w, p, q) under external load cases. These two different types of parameters determine different forms of cable displacement, respectively, which will be explained below.

When considering the stiffness of the pylon and backstays, two linear or nonlinear lateral springs with stiffness coefficients k_a and k_b , as shown in Fig. 2, can be added in the model by replacing span $2a$ with $2a - H(\frac{1}{k_a} + \frac{1}{k_b})$, and H is an additional horizontal component of cable tension owing to the applied load. In this way, the deformed configuration of the cable with unmovable, movable or

elastic yielding supports subjected to vertical distribution can be obtained.

2.2. Compatibility equation for a cable

In order to determine f_1 and f_2 in Eq. (3), the compatibility requirement that the unstressed cable length remain the same under different load cases can be used.

The cable's total length after stretching under external load s is determined by the following equation:

$$s = \int \sqrt{1 + \left(\frac{dy}{dx}\right)^2} dx \quad (4)$$

For cables with a maximum inclination of approximately 0.8 ($dy/dx < 0.8$), the following approximation can be applied [24]:

$$s = \int \sqrt{1 + \left(\frac{dy}{dx}\right)^2} dx \approx \int \left[1 + \frac{1}{2} \left(\frac{dy}{dx}\right)^2\right] dx \quad (5)$$

Total elongation Δs is given by

$$\begin{aligned} \Delta s &= \int_0^l \varepsilon(x) \frac{\partial s}{\partial x} dx = \int_0^l \frac{H}{EA} \sqrt{1 + \left(\frac{dy}{dx}\right)^2} \frac{\partial s}{\partial x} dx \\ &= \frac{H}{EA} \int \left[1 + \left(\frac{dy}{dx}\right)^2\right] dx \end{aligned} \quad (6)$$

The cable's unstressed length s_0 under the dead load and the live load, as well as the compatibility equation, can be expressed as

$$s_0 = s_d - \Delta s_d = s_l - \Delta s_l$$

where s_d and Δs_d represent the cable's total length and elongation length under the dead load, respectively; s_l and Δs_l represent the cable's total length and elongation length under the live load, respectively.

According to the compatibility equation, the sag of the cable at mid-span can be calculated based on the given live load.

2.3. Calculation of the cable's deformed sag at mid-span

According to Eqs. (5) and (6) and the compatibility requirement, f_1 and f_2 can be calculated by the following equations:

- (i) For load case 1

$$\begin{aligned} a \left[1 + \frac{2}{3} \left(\frac{f_1}{a}\right)^2\right] - \frac{(w+p)a^2}{EA} \left(\frac{a}{2f_1} + \frac{2f_1}{3a}\right) \\ = a \left[1 + \frac{2}{3} \left(\frac{f}{a}\right)^2\right] - \frac{wa^2}{EA} \left(\frac{a}{2f} + \frac{2f}{3a}\right) \end{aligned} \quad (7)$$

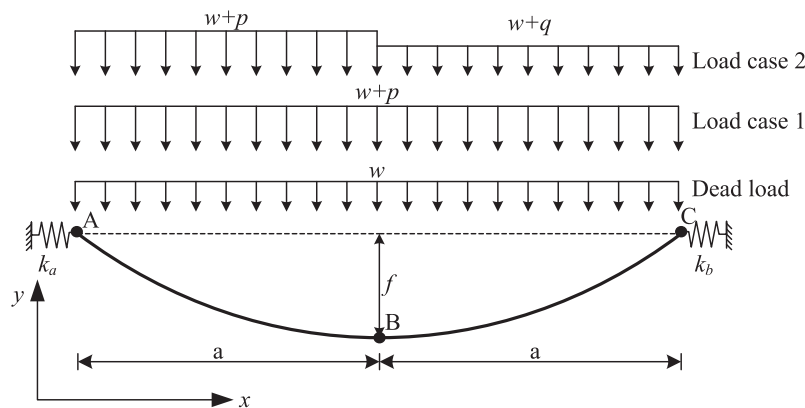


Fig. 2. Single cable parameters and three load cases.

The left side is the unstressed length of cable under load case 1, and right side is the length of the cable under the dead load, assuming that the influence of the stiffness of the pylon and backstays is neglected, and no movements at the top of the pylons. A cubic equation can be obtained by rearranging Eq. (7):

$$\left(\frac{f_1}{a}\right)^3 - \frac{(w+p)a}{EA} \left(\frac{f_1}{a}\right)^2 + \left[\frac{wa}{EA} \left(\frac{f}{a} + \frac{3a}{4f}\right) - \left(\frac{f}{a}\right)^2\right] \frac{f_1}{a} - \frac{3(w+p)a}{4EA} = 0 \quad (8)$$

(ii) For load case 2

$$\frac{1}{3} \frac{16w^2 + 16wp + 16wq + 6pq + 5p^2 + 5q^2}{a(p+q+2w)^2} f_2^2 - \frac{1}{6} \frac{(16w^2 + 16wp + 16wq + 6pq + 5p^2 + 5q^2)a}{EA(p+q+2w)} f_2 - \frac{(p+q+2w)a^3}{2EAf_2} = \frac{4a}{3} \left(\frac{f}{a}\right)^2 - \frac{2wa^2}{EA} \left(\frac{a}{2f} + \frac{2f}{3a}\right) \quad (9)$$

The following equation can be obtained by rearranging Eq. (9):

$$\frac{1}{3} \frac{C_1}{C_2^2} \left(\frac{f_2}{a}\right)^3 - \frac{wa}{6EA} \frac{C_1}{C_2} \left(\frac{f_2}{a}\right)^2 + \left[\frac{wa}{EA} \left(\frac{a}{f} + \frac{4f}{3a}\right) - \frac{4}{3} \left(\frac{f}{a}\right)^2\right] \frac{f_2}{a} - \frac{wa}{2EA} C_2 = 0 \quad (10)$$

where

$$C_1 = 16 + 16\frac{p}{w} + 16\frac{q}{w} + 6\frac{pq}{w^2} + 5\left(\frac{p}{w}\right)^2 + 5\left(\frac{q}{w}\right)^2$$

$$C_2 = \frac{p}{w} + \frac{q}{w} + 2$$

From Eqs. (8) and (10), the mid-span sag in the two load cases, f_1 and f_2 , can be obtained. The deformed cable configurations are given by Eq. (3). The stress can be determined according to the cable configuration functions and horizontal force H .

2.4. Deformation behaviors of single-cable structures

As we know, for a single-span simply supported beam, the maximum displacement occurs at the time when the external loads acts on the entire span of the bridge (load case 1, LC1, as shown in Fig. 2). However, there are certain distinctions for cable structures. In contrast to frame structures, the deformation of the cable structures, including elastic deformations and non-straining (kinematic) deformations, consists of two parts. Under different load cases, different type of deformations controls the total displacements. Kinematic deformations are caused by initial shape change of the cable, resulting from local or asymmetric loads, such as load case 2 (LC2, as shown in Fig. 2). To more clearly illustrate the deformation behaviors of single-cable structures, and determine the controlling load cases for cable-truss structures, some parametric analysis for a single cable structure were carried as figured in Fig. 3. The geometric, material and load parameters of a single cable are illustrated in the figures.

It is not difficult to find that the cable will keep its parabolic shape, and only the mid-span sag has changed under external load based on Eq. (3.1). However, different from load case 1, from Eq. (3.1), the cable does not keep its initial parabolic shape anymore, and the final configuration is depended on the load conditions and new mid-span sag under load case 2. According to the derivations of the new mid-span sag under two load cases, the mid-span sag can only be determined by the elastic deformation because Eqs. (8) and (10) were derived from the cable's unstressed length. Therefore, the change of mid-span sag, which reflects the elastic deformations and the bridge configuration, can be

determined by the load parameters, which are proportional to mid-span sag.

Fig. 3a shows that the structure's deflection decreases as sag-span ratio f/l increases. It means that a cable structure with a large sag-span ratio is stiffer than one with a small sag-span ratio under LC1. However, the opposite is true under LC2, and the structure deflection is far larger under LC2 compared to LC1, even though the external load acting on the structure in LC2 is smaller than that in LC1, as shown in Fig. 3b. It is because the elastic deformation controls the cable structure's deflections under LC1. Fig. 3a also shows that the changes of the mid-span sag are very small compared to their initial mid-span sag, even though the live load is 2.5 times of the dead load. As described above, under load case 2, the cable's deformation is determined by the load parameters, and it is proportion to mid-span sag. From Eq. (3.1), it is easy to find that the cable displacement is only determined by the final mid-span sag when the cable is subjected to the same load. It has been proved that the change of the mid-span sag is very small under external load, and it may be neglected compared to their initial mid-span sag from Fig. 1a. Therefore, under the same asymmetric loads, the deflection is proportional to the cables' initial mid-span sag. This is the reason that the results shown in Fig. 3b show an increase in structure deflection as sag-span ratio f/l increases. From another perspective, the cable is longer when the sag-span ratio is larger, and it is easier to deform and have large displacement. Finally, it is obvious that the deflection under LC2 is the main factor that controls the cable's structure stiffness design, whereas the stress/force under LC1 controls the cable structural strength design according to Eq. (1).

Fig. 3c shows the cable's deflection with different q . The magnitude of q has a significant influence on the cable's deflection. When $k = 0$, the deflection curve is the same as the curve in Fig. 3b, with $f/l = 1/10$. When $k = 1$, the deflection curve is the same as the curve in Fig. 3a, with $f/l = 1/10$. Compared to $k = 0$, the maximum

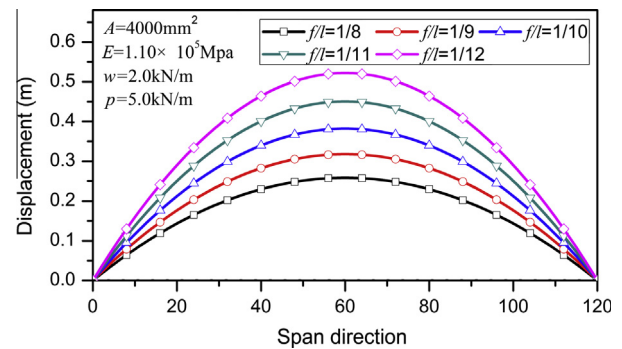


Fig. 3a. Deflection curves under LC1.

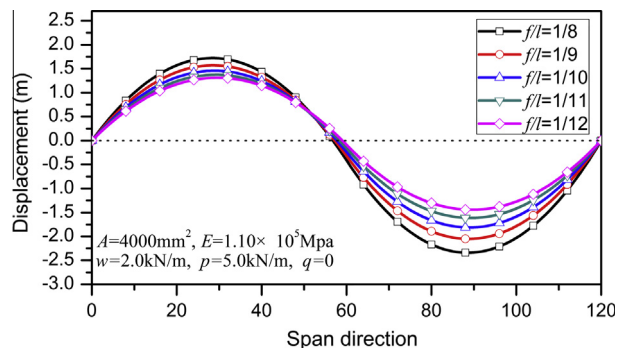


Fig. 3b. Deflection curves under LC2 when $q = 0$.

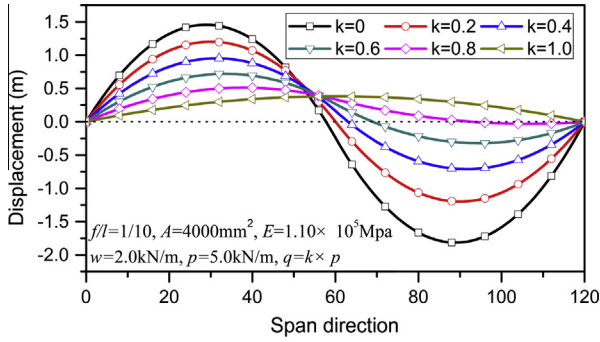


Fig. 3c. Deflection curves under LC2 with different q .

displacement decreases by 66%, 53%, 40%, 0.28%, and 0.21% when $k = 0.2, 0.4, 0.6, 0.8,$ and 1.0 , respectively. It can be concluded that q can effectively reduce the cable's deformation and displacement. However, for most cable structures, e.g., single-cable structures and traditional suspension bridges, k is always chosen close to 0 under LC2, this is because that its influences on the girder's stiffness and the horizontal displacement of the hangers are limited.

3. Mechanics model for cable-truss footbridges

For the cable-truss footbridge shown in Fig. 1, the two cable systems are the main load-bearing members, and the vertical stiffness of the deck system, which is usually made of thin steel plates, can be neglected. The main cable undertakes the total dead load of the bridge, including the weight of the deck system and the two cable systems; the initial tension, which guarantees the deck cable's initial configuration under the bridge finished state, also acts on the main cable through hangers. The live load can be assumed acting on the deck cable directly, and then applied on the main cable through the hangers' tension. Therefore, the mechanics model of the cable-truss footbridge is actually a tension-tension mechanical system combining the stiffness of the main cable and that of the deck cable. Before proceeding to the derivation, the following two assumptions are made in addition to the assumptions for single cable.

- (3) The hangers form a uniform curtain suspended between the main cable and deck cable, and the hangers are inextensible. It means that the cables are only subjected to vertical load, and the horizontal deformation is not considered in the following derivations. Even though the use of inclined hangers may stiffen the cable-truss structures significantly, the mechanics model proposed here is not really suitable to deal with that effect, because of the simplifications on cables' mechanical properties under horizontal loads. In that case, it is best to resort directly to finite element method.
- (4) The deck system is a local load-bearing member; and only its vertical stiffness is considered in the derivations.

According to Eq. (2), the main cable and deck cable under the bridge finished state (dead load case) can be expressed as follows:

$$y_w^m = \frac{f_w^m}{a^2} x(x - 2a) \quad (11)$$

$$y_w^d = -\frac{f_w^d}{a^2} x(x - 2a) \quad (12)$$

where f_w^m and f_w^d denote the design sag at the mid-span of the main cable and deck cable, respectively, under the uniform dead loads w_m and w_d , respectively.

The following relationship between w_m and w_d can be found under the bridge finished state:

$$w_m = w_{deck} + w_{cm} + w_{cd} + w_t \quad (13)$$

where w_{deck} denotes the weight of the deck system; w_{cm} and w_{cd} represents the self-weight of the main cable and the deck cable, respectively; w_t is the deck cable's initial tension to guarantee the deck cable's initial configuration under the bridge finished state, and is equal to w_d . Hereafter, w_d is substituted by w_t to describe the initial tension acting on the deck cable under the bridge finished state.

3.1. Deformation analysis

Similar analysis has been conducted by Huang et al. [17] using FEM analysis. In this section, we shall conduct a deformation analysis based on the proposed mechanics model, which includes the case of the semi-span loads that were not considered by Huang et al. The mathematical formula for the cable-truss bridge deformation under full-span and semi-span loads are derived based on the single cable theory and an iterative method. When the derivation involves the deck cable, for simplicity and convenience, we can reverse the deck cable's profile, and load analysis can be done by using the same coordinate systems as that of the main cable when the derivation involves the deck cable.

3.1.1. Deformation under load case 1

Under load case 1, there is a uniform load p acting on the total span. The two cable profiles under load case 1 are expressed as

$$y_1^i = \frac{f_1^i}{a^2} x(x - 2a) \quad (i = m, d) \quad (14)$$

where superscript $i = m$ denotes the main cable, and d refers to the deck cable when $i = d$; the external load p sustained by the main cable is p_m , and that for the deck cable is p_d ; $p = p_m - p_d$.

According to Assumption 3, the relative displacement of the main cable and the deck cable is 0, and hence,

$$\delta(x) = y_1^m - y_w^m = y_1^d - y_w^d \quad (15)$$

where $\delta(x)$ is the bridge deflection function.

By substituting Eqs. 11, 12, and 14 into Eq. (15), the following equation can be derived:

$$\frac{f_1^m - f_w^m}{a^2} x(x - 2a) = -\frac{f_1^d - f_w^d}{a^2} x(x - 2a) \quad (16)$$

Therefore to calculate live load p carried by the main cable and deck cable, only the condition $f_1^m - f_w^m = -(f_1^d - f_w^d)$ needs to be satisfied.

By solving Eq. (8) for a given initial p_m or p_d , the sag of the cable at mid-span under load case 1 can be obtained, and the iterative method can be utilized to guarantee the agreement of Eq. (16). After completing these procedures, the deformation function $\delta(x)$ for the bridge can be calculated from Eq. (15).

3.1.2. Deformation under load case 2

As shown in Fig. 4, in contrast to load case 1, the force under load case 2 will produce upward displacement in the unloaded region, which will change hangers' tensile forces. q denotes the tension in the hangers produced by the external force in the unloaded region, and p_m and p_d are the same as in load case 1.

According to Eq. (4), under load case 2, the cable configuration can be expressed as

$$y_2^m = \begin{cases} \frac{2(p_m + w_m)x^2 - (3p_m + q_m + 4w_m)ax}{(p_m + q_m + 2w_m)a^2} f_2^m & (0 \leq x \leq a) \\ \frac{2(q_m + w_m)x^2 - (5q_m + 4w_m - p_m)ax - 2(p_m - q_m)a^2}{(p_m + q_m + 2w_m)a^2} f_2^m & (a < x \leq 2a) \end{cases} \quad (17)$$

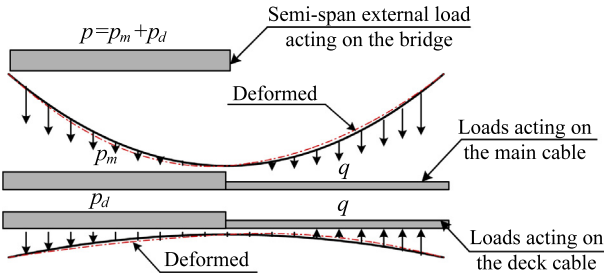


Fig. 4. Cable-truss footbridge's deformation under load case 2 (arrows represent the direction of internal forces).

$$y_2^d = \begin{cases} -\frac{2(p_d+w_d)x^2-(3p_d+q_d+4w_d)ax}{(p_d+q_d+2w_d)a^2} f_2^d & (0 \leq x \leq a) \\ -\frac{2(q_d+w_d)x^2-(5q_d+4w_d-p_d)ax-2(p_d-q_d)a^2}{(p_d+q_d+2w_d)a^2} f_2^d & (a < x \leq 2a) \end{cases} \quad (18)$$

The deformation equations of the cables are

$$y_2^m - y_w^m = \begin{cases} \frac{[2(p_m+w_m)f_2^m - (p_m+q_m+2w_m)f_w^m]x^2 - [(3p_m+q_m+4w_m)f_2^m - 2(p_m+q_m+2w_m)f_w^m]ax}{(p_m+q_m+2w_m)a^2} & (0 \leq x \leq a) \\ \frac{[2(q_m+w_m)f_2^m - (p_m+q_m+2w_m)f_w^m]x^2 - [(5q_m+4w_m-p_m)f_2^m - 2(p_m+q_m+2w_m)f_w^m]ax - 2(p_m-q_m)f_2^m a^2}{(p_m+q_m+2w_m)a^2} & (a < x \leq 2a) \end{cases} \quad (19)$$

$$y_2^d - y_w^d = \begin{cases} -\frac{[2(p_d+w_d)f_2^d - (p_d+q_d+2w_d)f_w^d]x^2 - [(3p_d+q_d+4w_d)f_2^d - 2(p_d+q_d+2w_d)f_w^d]ax}{(p_d+q_d+2w_d)a^2} & (0 \leq x \leq a) \\ -\frac{[2(q_d+w_d)f_2^d - (p_d+q_d+2w_d)f_w^d]x^2 - [(5q_d+4w_d-p_d)f_2^d - 2(p_d+q_d+2w_d)f_w^d]ax - 2(p_d-q_d)f_2^d a^2}{(p_d+q_d+2w_d)a^2} & (a < x \leq 2a) \end{cases} \quad (20)$$

In Eqs. (19) and (20), q_m and q_d represent the loads acting on the main cable and the deck cable respectively, and they are equal to the hangers' tension, q .

In order to satisfy Assumption 3, the two piecewise deformation functions should be compatible, which means that the five coefficients of the two functions must be equal, so there are five constraints to be fulfilled. However, there are only two variables, p_m (p_d) and q , in the two functions for the cable sag obtained from Eq. (10). First, assuming the deformation functions of the two cables are compatible in the loaded region, the following equation with respect to p_m and q can be derived:

$$\begin{cases} \frac{2(p_m+w_m)f_2^m - (p_m+q_m+2w_m)f_w^m}{(p_m+q_m+2w_m)} + \frac{2(p_d+w_d)f_2^d - (p_d+q_d+2w_d)f_w^d}{(p_d+q_d+2w_d)} = 0 \\ \frac{(3p_m+q_m+4w_m)f_2^m - 2(p_m+q_m+2w_m)f_w^m}{(p_m+q_m+2w_m)} + \frac{(3p_d+q_d+4w_d)f_2^d - 2(p_d+q_d+2w_d)f_w^d}{(p_d+q_d+2w_d)} = 0 \end{cases} \quad (21)$$

Using the iterative method, p_m and q can be obtained, and the corresponding sags of the two cables, f_2^m and f_2^d , can also be calculated according to Eq. (10). Because both equations in Eq. (21) are quadratic equations, so they have multiple roots, and one of them is the real. Therefore, the choice of the root of the equations is very important. When a bridge is reasonably designed, the parameters f_2^m and f_2^d should be very close to the parameters f_w^m and f_w^d respectively, and this characteristic can be used as a criterion to select the real root for Eq. (21).

Since Eq. (21) neglects the deformation compatibility condition in the unloaded region, whether the compatibility condition is satisfied or not should be discussed separately. Both the deformed and un-deformed bridge profile functions are continuous functions, and it is obvious that the deflection functions expressed in

Eqs. (19) and (20), composed of two piecewise parabolic functions, are also continuous. For unloaded region $[a, 2a]$, $x = a$ is also included in region $[0, a]$, and the deflection functions are continuous; therefore, the compatibility condition at $x = a$ is satisfied. The two cables are fixed at $x = 2a$ and their displacement is 0, so that the compatibility condition is automatically satisfied. In other words, the compatibility conditions are satisfied at the two boundary points, $x = a$ and $x = 2a$.

For a parabolic function, when the two boundary points are satisfied, only the third supererogatory condition that determines the parabolic function's quadratic term coefficient is needed to determine its profile. From Eqs. (19) and (20), the quadratic term coefficient of the displacement function in region $[a, 2a]$ can be expressed by the two coefficients of the displacement functions in region $[0, a]$, i.e., two times the linear term coefficient minus three times the quadratic term coefficient. Hence, the deformation compatibility condition is also satisfied on the unloaded area by using Eq. (21), even though it is only established on the loaded area.

3.2. Internal force and stress analysis

To this end, the deformation functions for the cable have been obtained. The moment $M(x)$ of the simply supported beam with the same span shown in Eq. (1) can be calculated easily according the total external load acting on the beam. The horizontal component of the cable's tension, H , will be obtained according to Eq. (1), and the cable tension $N(x)$ can be calculated by the following equation:

$$N(x) = H \sqrt{1 + \left(\frac{dy}{dx}\right)^2} \quad (22)$$

Subsequently, the stress can be calculated based on $N(x)$, by dividing $N(x)$ with the effective cross-section of cable A .

4. Verification of the proposed model

To investigate the reliability and accuracy of the proposed structural mechanics model, comparisons between the proposed model and the finite element model (FEM) have conducted. The structural parameters used in the comparison tests are chosen from a planned double-cable planed cable-truss bridge with a span of 120 m and a width of 2 m. The spacing of the hangers is 2 m, and the bridge deck is made of steel plates in the longitudinal direction and flange beams in the transverse direction. According to the design, the dead load in the deck system is only 1.8 kN/m, and the crowding load is 2.5 kN/m². The main cable is made of wire cable, whose tensile strength and elastic modulus are 1570 MPa and 1.10×10^5 MPa respectively. The bridge deck slope is 5%, which means the sag-span ratio of the deck cable is 1/40. In the

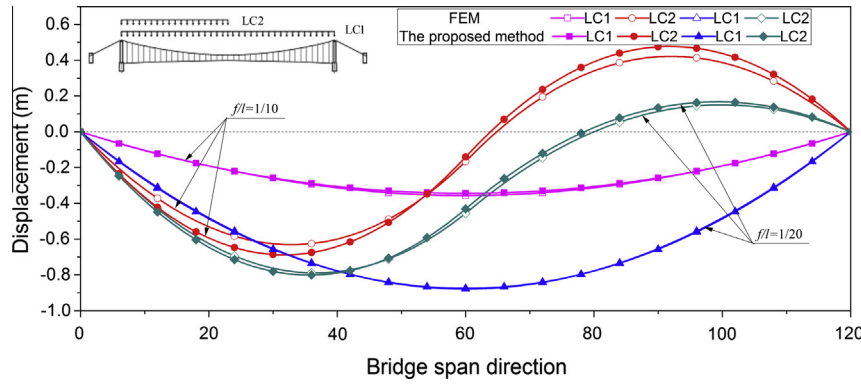


Fig. 5. Comparison of vertical deflection calculated by the FEM and the proposed method.

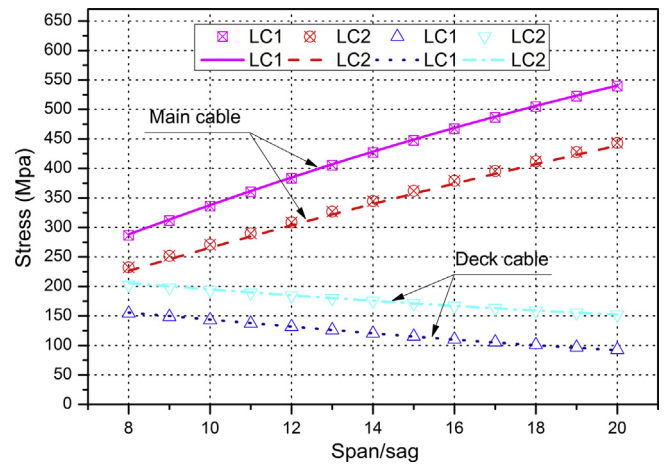
calculations, the effective cross-section of the main cable and deck cable are 2000 mm² and 2500 mm² respectively. These material model and load model parameters will also be used in Section 5.

The FEM analysis was conducted by using ANSYS, and the main and deck cables were divided by the 59 hangers into 60 elements. Link10 element supplied by ANSYS was used to model the cables and hangers, and the element's tension-only option was activated. The initial strain for each link element is calculated from the dead load and initial cable configuration. The weight of the deck system was modeled by Mass21. There are total 161 nodes and 240 elements in the FE model, and the larger displacement option was opened before the calculations.

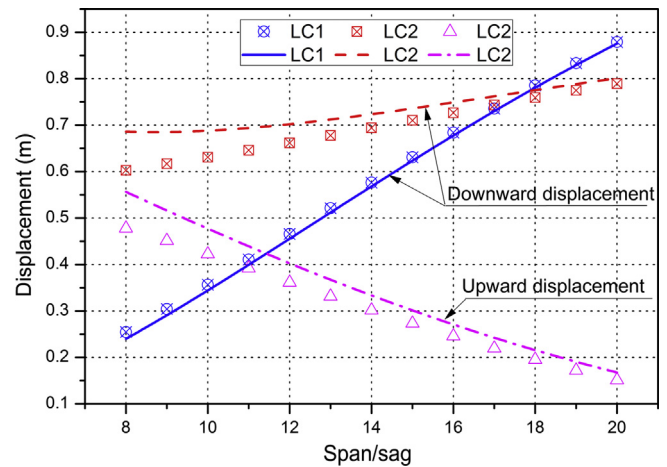
Fig. 5 shows the deflection curves of the bridge with a sag–span ratio of 1/10 and 1/20 under both LC1 and LC2. The deformation curves calculated by using the proposed structural mechanics model agrees well with those calculated by using the FEM under load case 1 (LC1). Under load case 2 (LC2), the deformation curves do not agree well with the FEM calculations; however, the differences between the two methods are within the allowable range. There are two main reasons for these discrepancies. First, the load acting on the FEM model is with respect to the undeformed state, which ignores the second order effects of the external load on the load-acting region, whereas the proposed bridge model is with respect to the deformed state, which takes account the external load's second order effects. Second, the proposed bridge model ignores the hangers' lateral effect, which can reduce the cable's deformation; this is also the reason that the deformation calculated by the proposed method is larger than that of the FEM. More comparisons are presented in Fig. 6, Tables 1 and 2.

Fig. 6a shows the main cable and deck cable stress profile under load case 1 and load case 2. The results calculated by the proposed method agree very well with those of the FE analysis under both live load cases (in contrast to the displacement results illustrated in Fig. 6b) and dead load. In FE analysis, the displacement results have higher-order accuracy than that of stress, but in the proposed mathematical model for cable–truss bridges, the stress results have higher-order accuracy. The calculation of stress, expressed in Eq. (22), is dependent on both the structure deformation and the bridge's initial geometric configuration.

According to Figs. 5 and 6b, it can be concluded that the proposed method predicts larger sag–span ratio under load case 2, which is different from the conventional methods. The reason for this distinction is that the larger sag–span ratio and the larger deformation will occur under load case 2. From Fig. 6b, it can be seen that the deck's deflection displacement under load case 2 increases as sag–span ratio decreases. This finding is completely opposite to the traditional suspension bridges or single-cable



(a) Maximum cable stress



(b) Maximum displacement

Fig. 6. Comparison of the maximum cable stress and deck displacement with respect to different sag–span ratios (dots denote the FEM results, and lines denote the results calculated by the proposed method).

structures, and the following section will offer some explanations and insights to this problem based on parametric analysis.

Tables 1 and 2 show the cable's maximum stress value and displacement value, respectively, and one may find that the maximum difference occurs between the two methods under the load case 2. As listed in the two tables, the maximum difference rate

Table 1
Cable stress results under load case 2.

f/l	Maximum cable stress (MPa)			Maximum deck stress (MPa)		
	FEM	Proposed method	Difference (%)	FEM	Proposed method	Difference (%)
1/8	232.30	226.42	-2.60	202.35	205.47	1.52
1/9	251.67	246.11	-2.26	198.05	200.22	1.08
1/10	270.93	265.60	-2.00	193.55	195.04	0.77
1/11	289.93	284.78	-1.81	188.95	189.98	0.54
1/12	308.60	303.58	-1.65	184.35	185.04	0.37
1/13	326.88	321.95	-1.53	179.81	180.26	0.25
1/14	344.73	339.88	-1.43	175.36	175.64	0.16
1/15	362.15	357.35	-1.34	171.05	171.21	0.09
1/16	379.15	374.39	-1.27	166.90	166.97	0.04
1/17	395.73	391.00	-1.21	162.93	162.93	0.01
1/18	411.92	407.21	-1.16	159.14	159.11	-0.02
1/19	427.74	423.05	-1.11	155.55	155.50	-0.04
1/20	443.21	438.53	-1.07	152.16	152.09	-0.05

Table 2
Deck displacement results under load case 2.

f/l	Maximum downward displacement (m)			Maximum upward displacement (m)		
	FEM	Proposed method	Difference (%)	FEM	Proposed method	Difference r (%)
1/8	0.60	0.69	12.14	-0.48	-0.56	14.10
1/9	0.62	0.69	9.96	-0.45	-0.52	12.56
1/10	0.63	0.69	8.28	-0.42	-0.48	11.51
1/11	0.65	0.69	6.90	-0.39	-0.44	10.76
1/12	0.66	0.70	5.72	-0.36	-0.40	10.23
1/13	0.68	0.71	4.82	-0.33	-0.37	9.74
1/14	0.69	0.72	4.07	-0.30	-0.33	9.54
1/15	0.71	0.74	3.47	-0.27	-0.30	9.38
1/16	0.73	0.75	2.96	-0.25	-0.27	9.29
1/17	0.74	0.76	2.45	-0.22	-0.24	9.41
1/18	0.76	0.78	2.07	-0.20	-0.22	9.38
1/19	0.77	0.79	1.73	-0.17	-0.19	9.76
1/20	0.79	0.80	1.48	-0.15	-0.17	9.85

of the cable's stress is less than 2.6% under load case 2. The maximum difference rate for the deck's downward displacement is 12.14%, and that of upward displacement is 14.10%, when sag–span ratio is 1/8. For most sag–span models, the displacement difference rates are less than 10%. Considering the differences in the two methods' external load-acting patterns, these difference rates are acceptable. Generally speaking, the proposed cable-truss bridge model is reliable and accurate.

5. Parametric analysis

The biggest difference between the cable-truss footbridge and traditional suspension footbridges is that the former has a tensed deck cable. Using this method, the weight and stiffness of the bridge deck, which can only be designed as a local load-bearing member, can be reduced in order to save materials. On other side, the cable-truss footbridge transforms the traditional footbridge from a flexural system or flexural-tensile system to a pure tensile system, which is the most economical structural system. The tensed deck cable not only increases the main cable's initial/gravity stiffness, but also reduces the cable's displacement and deformation, which can be seen in Fig. 4. According to the mathematical expressions in static equilibrium calculations, the deck cable also undertakes the external load with the main cable together. In this section, the following two issues are discussed: (1) internal force distribution between the two cable systems; (2) optimal material usage of cable-truss bridges compared to the traditional suspension footbridges.

A bridge with the same structural parameters and materials as described in Section 4 is used to conduct the parametric analysis.

The deck cable's sag–span ratio remained unchanged at 1/40 to meet the bridge deck's longitudinal design requirement.

5.1. Internal force distribution between the two cable systems

In the design of a footbridge, the pedestrian crowd load is always known in advance. Therefore, in the parametric analysis, k_{dl} is defined as the ratio of the dead load to the live load, and w_d/w_{deck} is defined as the ratio of the deck cable's initial tension to the dead load of the deck system. Other structure and load parameters are the same as that in Section 4. To investigate the influence of w_d in-depth, the weights of the two cables are neglected in the parametric analysis.

Since it is easier to understand the deformation and stress state of a single cable than that of a cable-truss bridge, if the external load sustained by the main cable is known, it is often convenient to model the cable-truss bridge as a single-cable structure. We define two parameters, p_m/p and q/p_m , here to describe the external loads acting upon the main cable, and the bridge's structure characteristics, which are analyzed based on the single-cable model of the cable-truss bridge. As defined previously, p is the external load and p_m denotes the load carried by the main cable. q is the tension acting on the main cable in the unloaded region under LC2. It is obvious that p_m/p reflects the stiffness ratio between the main cable and deck cable. q/p_m may be regarded as a kinematic deformation reduction coefficient (the larger the q/p_m , the smaller the kinematic deformation). Reducing kinematic deformation is the second function or task of the deck cable under asymmetric loads; the first function is to enhance the structure's gravity stiffness.

According to the mechanics model for suspension bridges, Steinman’s stiffness factor α describes the ratio between the elastic stiffness of the stiffness girder and the gravity stiffness of the cable [3]. α is given as

$$\alpha^2 = \frac{EI}{Hl^2} \tag{23}$$

where EI is the vertical stiffness of the beam, H is the horizontal component of the cable’s force, and l is the span of the bridge. Similarly, k_G , a parameter for describing the gravity stiffness ratio between the main cable and deck cable for a cable-truss footbridge, can be defined as

$$k_G = \frac{H_m}{H_d} = \frac{\frac{w_m l^2}{8f_m}}{\frac{w_d l^2}{8f_d}} = \frac{w_m f_d}{w_d f_m} = \left(\frac{w_{deck}}{w_d} + 1 \right) \frac{f_d}{f_m} \tag{24}$$

where w_d represents the pre-stressed uniform tension of the deck system.

According to Eq. (24), it is not difficult to see that the deck cable’s stiffness increases faster than that of the main cable. And the same conclusion can be drawn from the numerical results, as shown in Figs. 7 and 8. In Fig. 7, the expression of k_{dl} is defined as

$$k_{dl} = \frac{w_{deck}}{w_{live}}$$

where w_{live} is the live load acting on the bridge, and is equal to $p = 5.0$ kN/m.

$f/l = 1/10$ is a commonly used sag–span ratio in traditional suspension bridge design, therefore the main cable sag–span ratio in the study of the cable–truss bridge’s mechanical behaviors with respect to w_d/w_{deck} was set at $1/10$.

It is worth mentioning that the stiffness and strength of the bridge are the two key factors in bridge design. These two factors, which must be balanced with economic considerations, should be addressed simultaneously. For the cable–truss bridge, k_{dl} and w_d/w_{deck} are small, so that the structure’s stiffness is small, and the displacement under live load cases will be large, which makes stiffness the controlling factor in design. Increasing k_{dl} and w_d/w_{deck} will increase the stiffness of the bridge, and more materials will be needed, leading to a strength controlling design.

As shown in Fig. 7a and Fig. 7b, under both LC1 and LC2, the p_m/p curves reveal the same trend. The external load sustained by the main cable decreases as w_d/w_{deck} increases, which means that the deck cable will carry a greater load when the initial tension in the hangers under the bridge finished state increases. The effective cross section areas of both cables can be used as parameters in design to adjust the bridge’s internal force distribution because the redundancy can enhance the cable load carrying capacity. Another

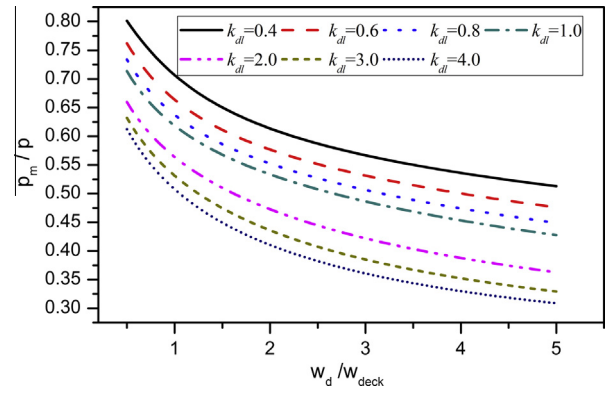


Fig. 7b. p_m/p under LC2 ($f/l = 1/10$).

notable result is that when w_d/w_{deck} remains constant as k_{dl} increases, which means that the bridge’s gravity stiffness increases when p_m/p decreases. Usually, the cable’s stress controls the design, as the gravity stiffness is large. However, when the load carried by the deck is greater, the deck cable’s section should be increased. A large sag–span ratio is more economical when the cable’s stress is the controlling factor in the design, but here the deck cable’s sag–span ratio is only $1/40$. This implies that the utility ratio of the main cable is low, and the cable–truss bridge is not suitable when the weight of the deck system is large, especially for cases when stress controls the design.

Fig. 7c illustrates that when dead-load-to-live-load ratio k_{dl} is less than 1.0, kinematic deformation reduction coefficient q/p_m increases as w_d/w_{deck} increases. For the main cable with a small k_{dl} , it is economical to increase the deck cable’s initial tension w_d , because the structure’s maximum displacement is significantly reduced compared with that of a single-cable structure with the same structural parameters. However, this advantage disappears when k_{dl} is larger than 1.0, especially for larger values of w_d/w_{deck} . From this perspective, the cable–truss bridge is only suitable when k_{dl} is small, meaning that stiffness controls the design.

In Figs. 8a and 8b, the relationship between gravity stiffness ratio k_G in Eq. (24) and w_d/w_{deck} is illustrated again. Therefore, Eq. (24) can be used to adjust the internal force distribution between the main cable and the deck cable by qualitatively modifying the deck cable’s initial tension.

According to the deformation analysis of single-cable bridge as shown in Fig. 3a, when w_d/w_{deck} and k_{dl} are the same, a main cable with a large sag–span ratio, f/l , will be stiffer than that with a small sag–span ratio under LC1. This is the reason why the curves in Fig. 8a declines as f/l decreases, because p_m/p reflects the stiffness

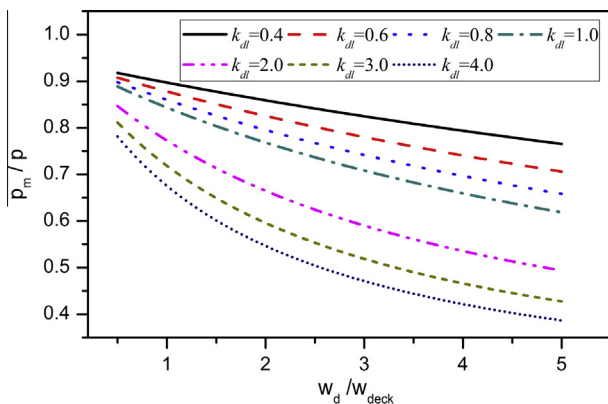


Fig. 7a. p_m/p under LC1 ($f/l = 1/10$).

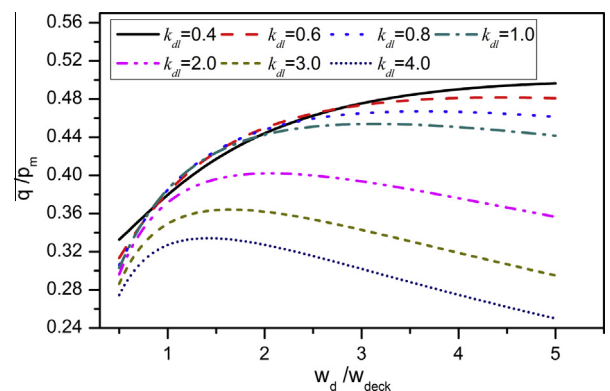


Fig. 7c. q/p_m under LC2 ($f/l = 1/10$).

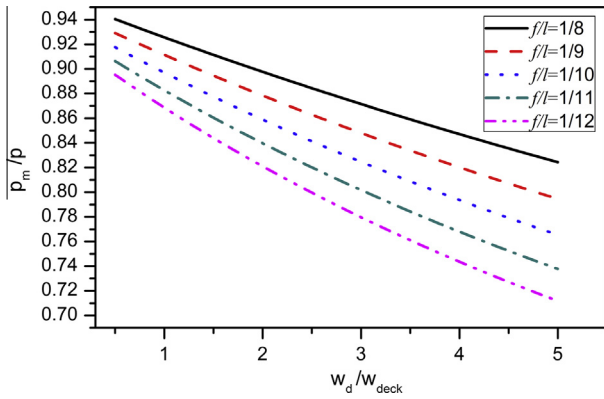


Fig. 8a. p_m/p under LC1 ($k_{d1} = 0.4$).

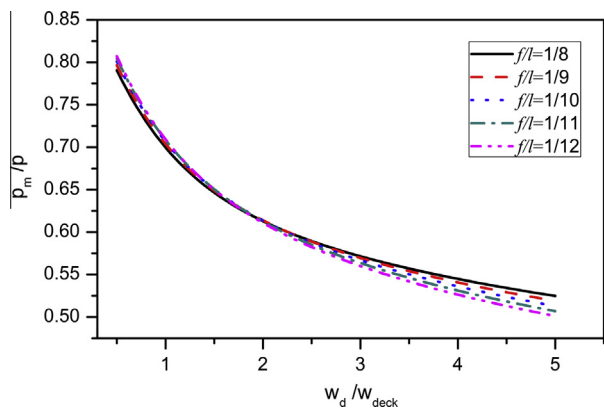


Fig. 8b. p_m/p under LC2 ($k_{d1} = 0.4$).

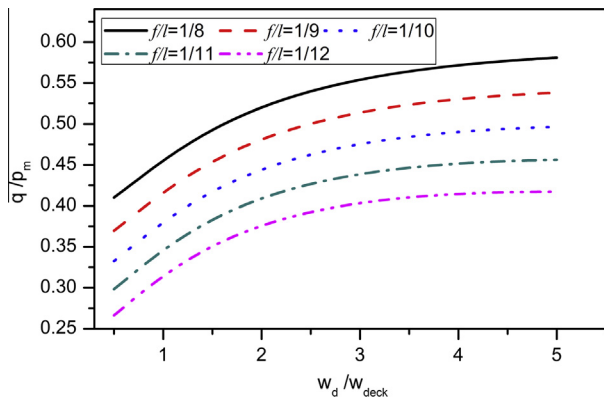


Fig. 8c. q/p_m under LC2 ($k_{d1} = 0.4$).

ratio between the main cable and the deck cable, and this is incompatible with Eq. (24), which only reflects the cable's gravity stiffness and neglects the elastic stiffness. Fig. 8b shows that the five curves almost coincide with each other, which implies that p_m/p is not sensitive to the main cable's sag-span ratio. However, Fig. 8c illustrates that the larger sag-span ratio f/l is, the greater the q/p_m is. Combining Fig. 8b and Fig. 8c, it can be observed that the cable-truss structures' maximum displacement increases as the main cable's sag-span ratio decreases under LC2. This phenomenon has already been described in Section 4, but it is explained here. From Fig. 6b, it is easy to see that influenced by the deck cable the structure's maximum displacement decreases as the main

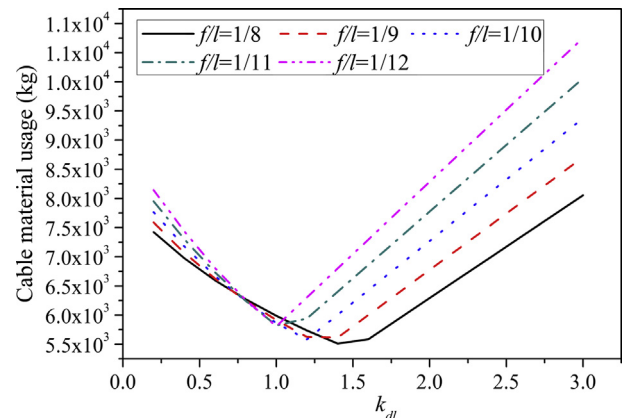
cable's sag-span ratio increases under semi span loads, and this is entirely different from the traditional suspension bridges.

Fig. 8 illustrates that a main cable with a large sag-span ratio is always stiffer than one with a small sag-span ratio under both LC1 and LC2. Eq. (24) can be used to adjust the external load distribution between the main and deck cables when the cable-truss bridge's geometrical and material parameters are the same. However, when a bridge has different sag-span ratios, Eq. (24) is no longer applicable. The relationship between the maximum displacement and sag-span ratio are different from that of the traditional suspension bridge. The cable-truss bridge with larger main cable sag-span ratio always obtains smaller maximum displacement under external load. Therefore, a larger main cable sag-span ratio is recommended, when the stiffness of the bridge is the main concern of the design.

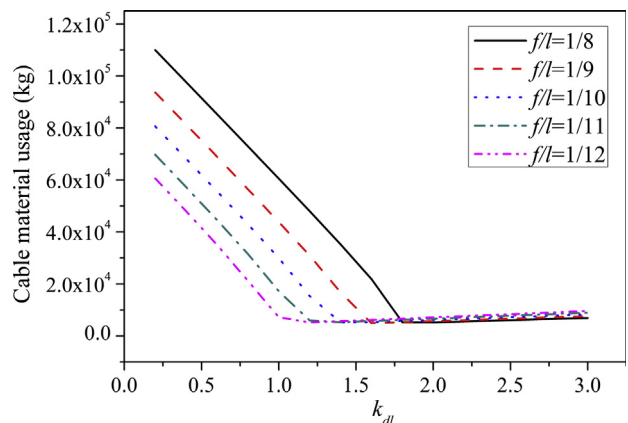
In the following section, a qualitative analysis that involves with the bridge's economic considerations obtained from Figs. 7 and 8 is performed using a structural optimization method.

5.2. Optimal cable material usage analysis

Generally speaking, the main cable is the most important load-bearing member for a suspension bridge. The bridge's stiffness is derived mostly from the gravity stiffness of the main cable. Therefore, the suspension bridge may be viewed as a single-cable structure in conceptual analysis. In this section, the optimal cable material usage of the proposed cable-truss bridge model and that



(a) Cable-truss structure



(b) Single-cable structure

Fig. 9. Optimal cable material usage of the cable with different sag-span ratio and k .

of a single-cable structure with the same span and under the same crowding load are compared. Before the analysis, the ratio between the dead load and live load is defined as k . The main cable's safety factor is 4.0, and the maximum structural displacement is $\leq L/150$. For the cable-truss bridge, the unstrained cable length of the deck cable equals the span of the bridge (120 m); therefore, equivalent initial tension w_t can be calculated by Eq. (25). The allowable stress for the cable is 250 MPa and the effective area of the deck cable is $\geq 500 \text{ mm}^2$.

$$w_t = \frac{64E_d A_d f_d^3}{16f_d^2 l^2 + 3l^4} \quad (25)$$

where E_d and A_d represent the elastic modulus and effective area, respectively, of the deck cable; f_d is the sag of the cable at mid-span, and l is the span of the bridge.

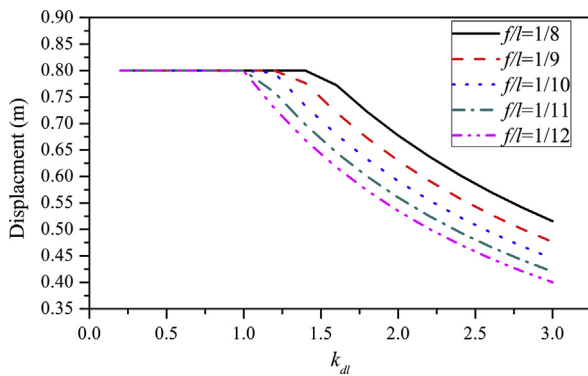
As shown in Fig. 9, there is an extreme point in each optimal material usage curve for both cable-truss structure and single-cable structure. Comparing the displacement and stress curves shown in Figs. 10 and 11, it is easy to find that when k_{dl} is small, the maximum displacement of the structure controls the design, so that more cables are needed to supply the stiffness to resist structure deformation under the live load (LC2). As k_{dl} increases, the gravity stiffness increases, and the stiffness demands from the cable decrease; therefore, the material usage of the cable shows a downward trend. However, these explanations are only adequate when the structure stiffness controls the design. After the extreme points as shown in Fig. 9, which corresponds to the same k_{dl} in Figs. 10 and 11, the cable stress controls the design, so that more cables are needed to reduce the cable's stress. This is the reason for the increase of the cable material usage curves in Fig. 9 after the inflection points. Fig. 9 also shows that the

cable-truss bridge with larger main cable sag–span ratio is always more economical.

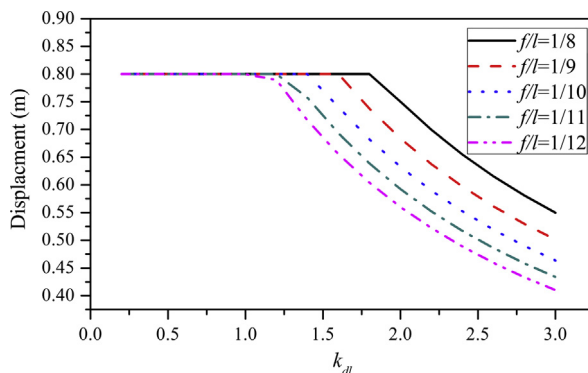
Comparing Figs. 9a and 9b, before the inflection point, the cable-truss bridge is much more economical than the single-cable structure, which is a good representative of traditional suspension footbridges. As listed in Table 3, when $k_{dl} = 0.2$ and $f/l = 1/10$, the steel cost of the single-cable bridge is 10.38 times that of the cable-truss bridge, and this multiplying factor will reach 14.81 when $k_{dl} = 0.2$ and $f/l = 1/8$. Due to the limited length of this paper, Table 3 only lists the optimal results of the effective area of the cables with a sag–span ratio of 1/8 and 1/10. For the planed bridge, the dead load is 1.8 kN, which means $k_{dl} = 0.36$, and the steel cost multiplying factor is about 10.0 when $f/l = 1/10$. Therefore, for a small value of k , the cable-truss bridge is a more feasible option than the traditional suspension footbridge.

The reason for this feasibility is that for the cable-truss bridge its main cable gravity stiffness increases according to the magnitude of deck cable tension, and the deck cable can reduce the structure's deflection amplitude under LC2. In contrast, the single-cable structure has to increase its stiffness according to the cable's elastic stiffness and weight. The later method for increasing the stiffness of the structure is inefficient and expensive. This can be seen from Fig. 11b, in which the cable's stress is very small before the extreme point. However, the stress in Fig. 11a is close to the allowable stress.

According to Figs. 10 and 11, if the cable-truss bridge is adopted, the range of k_{dl} corresponding to the displacement-controlling region will be reduced, which means that the stiffness controlling region will shrink, especially for a large sag–span ratio. According to Table 3, in the stress-controlling region, the cable-truss bridge is

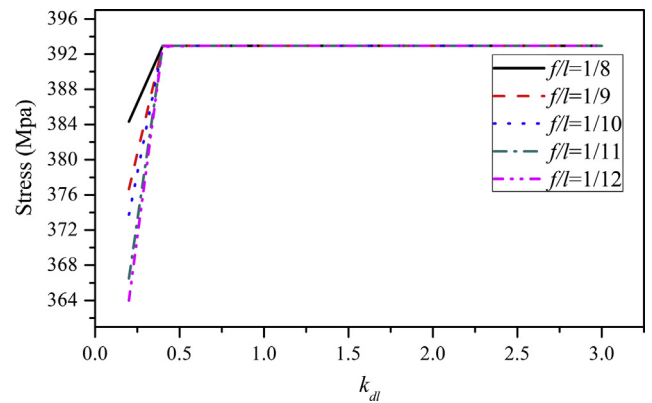


(a) Cable-truss structure

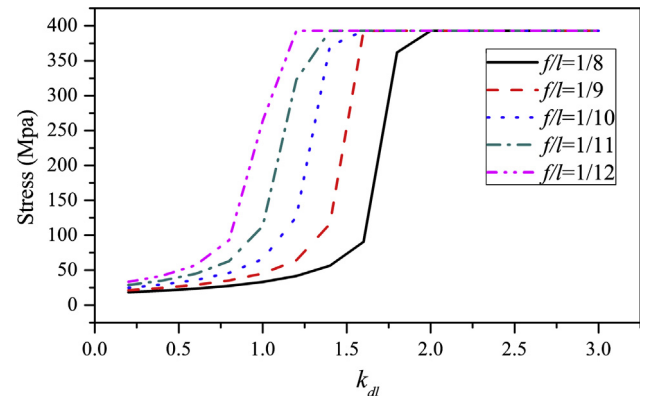


(b) Single-cable structure

Fig. 10. Maximum displacement under optimal solutions.



(a) Cable-truss structure



(b) Single-cable structure

Fig. 11. Maximum stress under optimal solutions.

Table 3
Partial optimal results of the effective areas of the cables (unit: mm²).

k_{dl}	$f/l = 1/10$			$f/l = 1/8$		
	Cable-truss structure		Single cable	Cable-truss structure		Single cable
	Main cable	Deck cable		Main cable	Deck cable	
0.2	1564.10	2431.52	40857.68	1299.03	2507.62	54954.85
0.4	1655.91	2033.14	34560.12	1415.30	2153.67	48799.83
0.6	1825.23	1596.32	28220.98	1560.97	1805.31	42633.40
0.8	1996.00	1196.56	21802.59	1707.14	1483.85	36449.70
1.0	2167.42	825.21	15196.22	1853.77	1183.51	30237.92
1.2	2342.32	500.00	7782.91	2000.80	899.98	23975.63
1.4	2556.71	500.00	2648.90	2148.20	630.20	17605.82
1.6	2770.83	500.00	2706.24	2310.34	500.00	10913.56
1.8	2984.72	500.00	2918.92	2486.79	500.00	2647.36
2.0	3198.44	500.00	3131.60	2663.13	500.00	2605.81
2.0	3412.03	500.00	3344.26	2839.38	500.00	2781.44
2.4	3625.49	500.00	3556.92	3015.56	500.00	2957.07
2.6	3838.87	500.00	3769.58	3191.67	500.00	3132.70
2.8	4052.16	500.00	3982.23	3367.73	500.00	3308.32
3.0	4265.38	500.00	4194.87	3543.75	500.00	3483.95

not as economical as the single-cable structure is. Therefore, without incurring the high cost needed to build pylons and anchoring systems, the cable-truss bridge is suitable for the case that the maximum displacement is the controlling factor in design, whereas the conventional types of bridges are often troubled by how to minimize the maximum displacement of the structure. In other words, the cable-truss bridge is recommended when the bridge's dead-load-to-live-load ratio is small, because in this situation, the bridge's gravity stiffness is small, and it may have large displacement under external loads. This is also the reason that the cable-truss bridge is recommended to be used as footbridge, which always has small dead-load-to-live-load ratio. However, the cable-truss bridge is not suitable for the case when the cable's strength is the controlling factor in the design.

6. Conclusions

In this paper, a simplified structural mechanics model for cable-truss footbridges is proposed for a fast and preliminary analysis in the bridge design. The model is derived based on the assumptions that the hangers are vertically arranged, and the stiffness of the deck system can be neglected. The reliability and accuracy of the proposed model have been validated by a systematic nonlinear finite element analysis. Based on the proposed mechanics modeling and corresponding parametric analysis, the main findings of the study are summarized as follows:

- (1) The proposed structural mechanics model for the bridge can be used as a simplified method in the conceptual/preliminary design of a cable-truss footbridge to determine the optimal structural parameters, and it is also an effective method for validating other approaches based on more complex models.
- (2) The pre-tension force of the deck cable can be used as a mechanism to adjust internal force distribution between the two cable systems. The larger the pre-tension force, the less the external force shared by the main cable under the same geometrical and material conditions.
- (3) Influenced by the deck cable, the maximum displacement of the structure decreases as the main cable sag-span ratio increases under semi span loads, which is entirely opposite to that of traditional suspension bridges. However, the semi span load case is still a maximum displacement-control load case. Therefore, a large main cable sag-span ratio is recommended when the maximum displacement of the cable-truss bridge does not meet the requirements.

- (4) According to the optimal cable material usage analysis, cable-truss bridge is far more economical than the traditional suspension bridge, because it does not need to consider the cost of pylons and anchoring systems, which is used to be the main option to reduce the maximum displacement of the bridge. It also reveals that a large main cable sag-span ratio is more suitable in this case.

Finally, the proposed model did not consider the transverse loads, and the human activities or/wind induced vibration that need to be investigated in future.

Acknowledgments

This research was supported by the National Natural Science Foundation of China (Grant No. 51078164), the National Basic Research Program of China (973 Program: 2011CB013800), and the National Natural Science Foundation of China for Distinguished Young Scholars (Grant No. 50925828). The authors would like to thank anonymous reviewers for their constructive comments and suggestions.

References

- [1] Fiore A, Monaco P. Pod-based representation of the alongwind equivalent static force for long-span bridges. *Wind and Struct*. 2009;12(3):239–57.
- [2] Buchholdt HA. An introduction to cable to cable roof structures. Cambridge: Press Syndicate; 1999.
- [3] Cobo del Arco D, Aparicio AC. Preliminary static analysis of suspension bridges. *Eng Struct* 2001;23:1096–130.
- [4] Ingólfsson ET, Georgakis CT. A stochastic load model for pedestrian-induced lateral forces on footbridges. *Eng Struct* 2011;33(12):3454–70.
- [5] Baron F, Venkatesan MS. Nonlinear analysis of cable and truss structures. *ASCE J Struct Div* 1971;97(2):679–710.
- [6] Ricciardelli F, Pizzimenti AD. Lateral walking-induced forces on footbridges. *J Bridge Eng* 2007;12(6):677–88.
- [7] Monforton GR, El-Hakim NM. Analysis of truss-cable structures. *Comput Struct* 1980;11(4):327–35.
- [8] Faridani HM, Barghian M. Improvement of dynamic performances of suspension footbridges by modifying the hanger systems. *Eng Struct* 2012;34:52–68.
- [9] Irvine HM. *Cable structures*. Cambridge: The MIT Press; 1981.
- [10] Taylor IJ, Vezza M. A numerical investigation into the aerodynamic characteristics and aeroelastic stability of a footbridge. *J Fluids Struct* 2009;25(1):155–77.
- [11] Schlaich J, Englesmann S. Stress ribbon concrete bridge. *Struct Eng Int* 1996;6(4):271–4.
- [12] Strasky J. Precast stress ribbon pedestrian bridges in Czechoslovakia. *PCI J* 1987;53–73. May–June.
- [13] Turmo J, Luco E. Effect of hanger flexibility on dynamic response of suspension bridges. *J Eng Mech* 2010;136(12):1444–59.
- [14] Santoso K. *Wide-span cable structures*. Massachusetts Institute of Technology; 2003.

- [15] Bruno L, Venuti F, Nasce V. Pedestrian-induced torsional vibrations of suspended footbridges: proposal and evaluation of vibration countermeasures. *Eng Struct* 2012;36:228–38.
- [16] Liao L, Du BS. Finite element analysis of composite truss structures containing pre-tensioned cable. In: *The 17th Annual International Conference on Composites/Nano Engineering (ICCE-17)*; July 26–31, 2009, Hawaii, USA.
- [17] Huang MH, Thambiratnam DP, Perera NJ. Load deformation characteristics of shallow suspension footbridge with reverse profiled pre-tensioned cables. *Struct Eng Mech* 2005;21(4):375–92.
- [18] Huang MH, Thambiratnam DP, Perera NJ. Vibration characteristics of shallow suspension bridge with pre-tensioned cables. *Eng Struct* 2005;27:1220–33.
- [19] Huang MH, Thambiratnam DP, Perera NJ. Dynamic performance of slender suspension footbridges. *J Sound Vib* 2007;303:239–54.
- [20] Huang MH, Thambiratnam DP, Perera NJ. Coupling coefficient and lateral vibration of slender suspension footbridges. *Comput Struct* 2008;86:27–37.
- [21] Majowiecki M. Structural architecture for large roofs: concepts and realizations. *Bautechnik* 2005;82(3):147–56.
- [22] Ali NBH, Rhode-Barbarigos L, Albi AAP, Smith IFC. Design optimization and dynamic analysis of a tensegrity-based footbridge. *Eng Struct* 2010;32:3650–9.
- [23] Carpineto N, Lacarbonara W, Vestroni F. Mitigation of pedestrian-induced vibrations in suspension footbridges via multiple tuned mass dampers. *J Vib Control* 2010;16(5):749–76.
- [24] Gimsing NJ. *Cable-supported bridges: concept and design*. 2nd ed. Chichester: Wiley; 1997.
- [25] Kmet S, Kokorudova Z. Nonlinear analytical solution for cable truss. *J Eng Mech* 2006;132(1):119–23.
- [26] Kmet S, Kokorudova Z. Nonlinear closed-form computational model of cable truss. *Int J Non-Linear Mech* 2009;44:735–44.
- [27] Law SS, Wu ZM, Chan SL. Vibration control study of a suspension footbridge using hybrid slotted bolted connection elements. *Eng Struct* 2004;26:107–16.
- [28] Nakamura S, Kawasaki T. A method for predicting the lateral girder response of footbridges induced by pedestrians. *J Constr Steel Res* 2009;65:1705–11.
- [29] Ureljus DE, Fowler DW. Behaviour of prestressed cable truss structures. *J Struct Div* 1974;100(8):1627–41.
- [30] Goremikins V, Rocens K, Serdjuks D. Decreasing displacement of prestressed suspension bridge. *J Civ Eng Manage* 2012;18(6):858–66.